The Conversion of Wollastonite to CaCO3 Considering Its Use for CCS Applications as Cementitous Material

Svensson, Kristoff; Neumann, Andreas; Feitosa Menezes, Flora; Lempp, Christof; Pöllmann, Herbert

applied sciences

MDPI

Article

The Conversion of Wollastonite to $CaCO_3$ Considering Its Use for CCS Application as Cementitious Material

Kristoff Svensson *, Andreas Neumann, Flora Feitosa Menezes, Christof Lempp and Herbert Pöllmann

Institute for Geosciences and Geography, Martin-Luther-University of Halle-Wittenberg, Von-Seckendorff-Platz 3, 06120 Halle (Saale), Germany; andreas.neumann@geo.uni-halle.de (A.N.); flora.menezes@geo.uni-halle.de (F.F.M.); christof.lempp@geo.uni-halle.de (C.L.); herbert.poellmann@geo.uni-halle.de (H.P.)

* Correspondence: kristoff.svensson@geo.uni-halle.de; Tel.: +49-345-55-26138

Received: 21 December 2017; Accepted: 8 February 2018; Published: 20 February 2018

Featured Application: Building materials and CCS.

Abstract: The reaction of wollastonite ($CaSiO_3$) with CO_2 in the presence of aqueous solutions (H_2O) and varied temperature conditions (296 K, 323 K, and 333 K) was investigated. The educts ($CaSiO_3$) and the products ($CaCO_3$ and SiO_2) were analyzed by scanning electron microscopy (SEM), powder X-ray diffraction (PXRD), and differential scanning calorimetry with thermogravimetry coupled with a mass spectrometer and infrared spectrometer (DSC-TG/MS/IR). The reaction rate increased significantly at higher temperatures and seemed less dependent on applied pressure. It could be shown that under the defined conditions wollastonite can be applied as a cementitious material for sealing wells considering CCS applications, because after 24 h the degree of conversion from $CaSiO_3$ to $CaCO_3$ at 333 K was very high (>90%). As anticipated, the most likely application of wollastonite as a cementitious material in CCS would be for sealing the well after injection of CO_2 in the reservoir.

Keywords: CCS; wollastonite; carbonation; CLUSTER; CS-cement; sealing

1. Introduction

To reduce the amount of CO_2 in the atmosphere (currently 403 ppm [1]) several possibilities need to be considered. One possible technology being investigated and discussed is carbon capture and storage (CCS). The goal of CCS is reducing CO_2 emissions from burning of fossil fuel by storing considerable amounts in suitable deep geologic reservoirs. The reservoirs considered for injection could be on- or offshore formations which could be in part already former exploited gas fields [2]. After injection, the sealing of wells in deep geologic formations being considered for CCS must be sustainable. Therefore, the choice of a tight and durable cement, used for sealing, is critical. The material has to resist the extreme conditions at the point of injection considering pressure, temperature, pH, and the composition of aggressive fluids (chloride rich brines, supercritical (sc) CO_2 accompanied with NO_2 and SO_2). The high amount of CO_2 and the fluids will have a considerable impact on cement properties. Hence, the term carbonation is occupied in the literature as a post hydration reaction of cementitious materials [3,4]. Ordinary Portland cements (OPC) cannot be used under these conditions of well boring due to their instability. The current study describes carbonation as a curing method to obtain carbonates as reaction products. In the present study, a literature review describing the influence of CO_2 on conventional hydrated cements as an alteration reaction is presented. Studies on the reaction of natural wollastonite with CO_2 as curing method under different pressures and temperatures were investigated.

Although natural deposits are limited, wollastonite can be fabricated using a conventional cement rotary kiln production process. Wollastonite has a Ca:Si ratio of 1:1 and therefore during production a better CO_2 balance than conventional cements with Ca:Si ratio 2:1 and 3:1 (Table 1, [5]).

Table 1. Raw meal CO_2-output of selected cement clinker phases. [5].

Phase	g of CO_2 per g Phase	Raw Materials
C_3S Alite	0.58	3 $CaCO_3/SiO_2$–OPC
C_2S Belite	0.51	2 $CaCO_3/SiO_2$
CS Wollastonite	0.38	$CaCO_3/SiO_2$
C_3A	0.49	$CaCO_3/Al_2O_3$
CA	0.28	$CaCO_3/Al_2O_3$
CA_2	0.17	$CaCO_3/Al_2O_3$
C_2F	0.32	$CaCO_3/Fe_2O_3$
C_2A	0.41	$CaCO_3/Al_2O_3$
C_4AF	0.36	$CaCO_3/Al_2O_3/Fe_2O_3$
C_3A_3Cs Sulfoaluminate	0.22	$CaCO_3/Al_2O_3/CaSO_4$

Additionally, the CO_2 will be consumed during the carbonation reaction thereby improving the CO_2 balance by forming carbonates.

The interaction of wollastonite and CO_2 [6] was investigated within the joint BMWi (German Federal Ministry for Economic Affairs and Energy) research project CLUSTER [7]. The project CLUSTER focusses on two main topics:

(I) Potential impacts of temporal variations in CO_2 stream composition and mass flow that occur in larger pipeline networks on transport, injection, and geological storage of CO_2.

(II) Flexibility of individual steps and the whole CCS process chain in response to this temporal variability [8].

In nature, wollastonite is formed during metamorphism. The present study considers the back reaction by carbonation of wollastonite forming $CaCO_3$ and SiO_2 as a base [6]. The carbonation reaction of wollastonite is described as extremely slow in absence of water at low temperatures [9]. Yet at 333 K and ambient pressure the $\overline{C}CS$ reaction is fast (several hours up to one day) in presence of water [9]. Microstructure aspects of the carbonation were investigated by Villani et al. [10] and Sahu and DeCristofaro [11]. Both studies showed a carbonation from the surface to the center of the wollastonite grains, similar to the shrinking core model [12]. Wollastonite reacts in the presence of CO_2 in aqueous conditions to calcite and amorphous silicon oxide:

$$CaSiO_3 + CO_2 \xrightarrow{H_2O} CaCO_3 + SiO_2(\text{amorphous}) \quad (1)$$

The chosen temperature (333 K) defined by the project CLUSTER [8] equates to the conditions in deep geological formations envisaged for CCS. Gartner and Hirao [9] and Longo et al. [13] found that the carbonation reaction strongly depends on the presence of water. Our experiments were performed under aqueous conditions, because aqueous solutions are expected to be present at the point of injection in wellbores.

1.1. Interaction of CO_2 and Conventional Hydrated Cements

Carbonation (i.e., formation of $CaCO_3$) in hydrated cements causes a decrease of the pH-value from approximately 13 to approximately 8. The calcium carbonate ($C\overline{C}$) mostly appears in form of calcite but also as vaterite and aragonite [3,4]. Carbonation is responsible for volume changes and formation of carbonates, hemicarbonates and monocarbonates, which leads to changes in porosity and permeability, and the formation of a fracture network. Dissolution of phases also may occur [3,4].

Considering the chemical and mechanical stability for construction due to changes of the porosity, this process is very critical [3,4].

Therefore, extensive research on the influence of CO_2 on OPC and wellbore cement was performed. Shi et al. [14] investigated the carbonation of white portland cement (wPc, CEM I 52,5 N) from Aalborg Portland A/S, Denmark, metakaolin (MK) and limestone (LS) mortars. Their mortars were hydrated for 91 days and exposed to a controlled atmosphere with one percent CO_2 at 293 K and 57% relative humidity (RH) for 280 days. They found that the Portland cement had the highest CO_2 binding capacity followed by limestone and metakaolin. Abdoulghafour et al. [15] and Luquot et al. [16] performed flow-through experiments with CO_2 and brine on fractured Portland cement. Their experiments were carried out at 333 K and 10 MPa for more than 100 h. They found that the leakage potential is controlled by the aperture of the fracture. Ozyurtkan and Radonjic [17] investigated the effect of CO_2 rich brine (two percent salt solution) on artificially fractured well-cement (class H) in a flow-through experiment over 30 and 100 days. After 100 days, a secondary fracture network was developed which was not present after 30 days. The secondary fractures caused higher leaching rates. The obtained data by Ozyurtkan and Radonjic [17] indicates a negative effect on porosity of cement under dynamic conditions which can be dependent on time. Yalcinkaya et al. [18], performed an experimental study on the dynamic alteration process of class-H wellbore cement caused by acidic brine. Their experiments confirmed leaching of Ca^{2+} from the reacted cement. Carey et al. [19] investigated the wellbore integrity and CO_2-brine flow along the casing-cement. They performed flow-through experiments at 313 K and 14 MPa pore pressure for 394 h. The brine was a 50:50 mixture of $scCO_2$ and 30,000 ppm NaCl-rich brine. They were able to confirm that degradation of Portland cement is slow. Barlet-Gouédard et al. [20] compared the behavior of a Portland cement with a Schlumberger CO_2 resistant cement (SCRC) with expanding agent under CO_2 geological storage environment (363 K, 28 MPa). They used brine containing 220 g/L NaCl. They focused on the expansion of the cement because fractures caused by the expansion are one possible occurrence of leakages. The simulated injection scenario presented by Barlet-Gouédard et al. [20] showed, that conventional Portland cement does not fulfill the requirements for the well integrity. Wigand et al. [21] performed flow-through experiments which simulated the diffusion of brine (1.65 M) and $scCO_2$ from the interface between wellbore cement and caprock into a fracture-bearing Portland cement. The experiments were performed at 327 K with a pore pressure of 19.9 MPa and a confining pressure of 26.2 MPa for 174 h. They showed that the carbonation of the wellbore cement at first caused closing and blocking of pores and fractures but opened other fractures in the following process, which increased the permeability. The chemical interaction along the cement–sandstone interface with $scCO_2$ was investigated by Nakano et al. [22]. They prepared a well composite sample consisting of casing, Portland cement and sandstone. The experiments were performed under 10 MPa and 323 K with a 0.5 M NaCl-brine. Their results indicate that the formation of carbonation layers act as a barrier to further CO_2-attack. Zhang et al. [23,24] investigated the reaction of two different pozzolan-amended (Class F fly ash, with ~70% silica, alumina and Fe_2O_3, ~5% sulfate, and less than 20% CaO) wellbore cements (API RP 10B; 35 vol % pozzolan and 65 vol % pozzolan) being exposed to CO_2 and H_2S gas mixtures and brine (one percent NaCl) at 323 K and 15.1 MPa for 2.5, 9, 28 and 90 days. The samples of the pozzolan-amended wellbore cement with 35 vol % pozzolan showed higher resistance against H_2S. Mito et al. [25] and Wolterbeek et al. [26] investigated the influence of CO_2-induced reactions on the mechanical behavior of fractured wellbore cement (class-G Portland cement). They found that the reaction with CO_2 did not produce further geomechanical weakening. In fact, samples with six weeks reaction time recovered peak-strength (83%) and increased frictional strength (15–40%). Kutchko et al. [27] investigated the reaction of hydrated well cement (class-H) with H_2S-CO_2 (21 mol % H_2S) acid-gas for 28 days at 323 K and 15 MPa. The H_2S added to the experimental setup resulted in significant formation of ettringite (interior region of the cement) and pyrite (carbonated rim of the cement). Although secondarily formed ettringite is known to cause cracking and strength loss, a mechanical damage caused by formation of ettringite was not found. Even the long-term

cement corrosion in chloride-rich solutions was investigated by Bube et al. [27]. They performed leaching experiments and thermodynamic simulations on cement (OPC; CEM I 32,5 R; w/c ratio of 0.4) with brine (4.3 mol Mg^{2+}, 0.41 mol Na^{+}, 0.54 mol K^{+}, 8.9 mol Cl^{-}, and 0.23 mol $SO_4{}^{2-}$) for 200 days. Comparing the results of laboratory and full-scale experiments, they were able to establish a link between the results of short-term laboratory experiments to long-term full-scale experiments, using thermodynamic equilibrium calculations.

The above research shows that carbonation can negatively impact the sealing qualities of OPC wellbore cements. Therefore, alternative materials are required to ensure wellbore integrity during the subsurface storage of CO_2. One such alternative is a cement based on wollastonite ($CaSiO_3$), which will create a seal through a carbonation reaction. In this study, experimental work addressing wollastonite carbonation kinetics under in-situ conditions relevant for subsurface CO_2 storage in aquifers or depleted reservoirs is presented.

1.2. Interaction of Wollastonite and CO_2

CO_2 has an impact on the stability of conventional hydrated cements. Therefore, the use of a cement, based on calcium silicate (CS) curing in the presence of CO_2 ($\overline{C}$), seems very promising [28–30]. Yet knowledge considering this approach is rather scarce.

Ashraf et al. [31] investigated the effects of high temperature (723–783 K) on calcium silicate-based cement (CSC), OPCs and OPCs with 20% fly ash. During the experiments, the OPCs showed a reduction of stiffness (60%), an increase of porosity (30%) and a loss of mass (13–15%) higher than the CSC (stiffness: 6%; porosity: 20%; mass loss: 3%). Huijgen et al. [32] investigated the mechanisms of aqueous wollastonite carbonation, using three different grain sizes (<38 µm, <106 µm and <500 µm) at short time intervals (5–60 min), a temperature range from 298 to 498 K and a pressure variation up to 4 MPa. A maximum conversion of 70% in 15 min at 473 K, 2 MPa CO_2 partial pressure and with a particle size of <38 µm was achieved. They were able to show that the aqueous carbonation mechanisms of wollastonite, steel slag and olivine are generally similar, although they showed that wollastonite carbonation was rapid, relative to the carbonation of Mg-silicates. Longo et al. [13] showed that water has a huge impact on the carbonation reaction of wollastonite. Without water the wollastonite sample carbonated on the surface rather fast but after a carbonate monolayer was formed, the reaction comes to a standstill. The presence of water completely changes the reaction and caused ongoing carbonation. Daval et al. [33] investigated the carbonation reactions of wollastonite at conditions relevant to geologic CO_2 sequestration in subsurface environments. They performed experiments in batch reactors at 363 K and 25 MPa. After carbonation, they found two reaction products: Calcite and a silica-rich phase. No other carbonate polymorph was found. Min et al. [34] performed carbonation experiments on wollastonite at typical geological storage conditions (333 K and 10 MPa). They investigated the microstructure of the carbonated wollastonite and found that after 20 h the reaction was controlled by the diffusion of water-bearing $scCO_2$ across the product layer on wollastonite surfaces. A layer of amorphous SiO_2 covered the surface of the wollastonite and functioned as a barrier.

2. Materials and Methods

To determine carbonation rates, several series of experiments were performed and different analytic techniques were applied. Educts and products were analyzed with powder X-ray diffraction (PXRD) and differential scanning calorimetry with thermogravimetry (DSC-TG) coupled with mass spectrometer (MS) and infrared spectrometer (IR). The chemical composition of the educts was analyzed with wave length dispersive X-ray fluorescence (XRF).

2.1. Materials

For the experiments, steel reactors with teflon liners from the company Büchi AG were used. According to the investigations of Huijgens et al. [32] (best conversion rate of 70% after 15 min at

473 K and 2 MPa) a sample material with a grain size <38 µm was chosen and the experiments were performed with 2 MPa. In this work, experiments at lower temperatures were performed because this work is connected to a specific CCS process, in which temperatures do not exceed 333 K. The used raw material (natural $CaSiO_3$, calcium silicate, meta, reagent grade, <20 µm powder) was supplied by Alfa Aeser. The chemical composition of the used raw material was analyzed with an XRF spectrometer (Siemens SRS 3000, Table 1). As expected the main elements were Si and Ca, but in addition the raw material contained small amounts of Fe, Al, Mg, Mn, Ti, K, and Sr (Table 2), which is due to the natural origin of this material.

Table 2. Chemical composition of the used raw material determined by Siemens SRS 3000.

Element (Oxides)	Content (wt %; Normalized)
SiO_2	50.55
CaO	45.95
Fe_2O_3	0.52
Al_2O_3	0.52
MgO	0.17
MnO	0.13
TiO_2	0.05
K_2O	0.03
SrO	0.01
LOI [1]	2.09
Total	100.02

[1] LOI: loss of ignition at 1323 K.

The pressure in the reactors was adjusted using an ISCO-pump (Teledyne ISCO, Model 500D Syring pump). CO_2 was supplied by Westfalen AG and had a purity of 4.5 (99.995%).

2.2. Analytical Methods

The mineralogical composition of the raw materials was measured by PXRD (Panalytical X'PERT^3 Powder with Pixcel 1D detector). The PXRD measurements were carried out with 45 kV and 40 mA. As apertures 0.04 rad soller slit and fixed slits (0.125° and 0.25°) were used. Diffractograms were recorded from 5° to 100° 2Θ with 49.725 s per step and stepsize: 0.013° 2Θ. For qualitative investigation the Highscore Plus Suite [35] and for quantitative phase analysis the Rietveld method [36] with Profex-BGMN [37,38] was used. To determine the amorphous content, 10 wt % rutile (Kronos 2900–TiO_2; Rutile, supplied by KRONOS TITAN GmbH, Leverkusen, Germany) was added as internal standard. Chemical composition was analyzed with wave length dispersive X-ray fluorescence (SRS 3000; Siemens, Karlsruhe, Germany; Rh-tube; vacuum: 200 mbar; measurement, 30 s for each line). Therefore, melting tablets with 1 g sample material and 8 g Di-Lithium Tetraborate (FX-X100-2) supplied by FLUXANA (Bedburg-Hau, Germany) were prepared.

To investigate the degree of carbonation depending on pressure (p) and temperature (T), the contents of wollastonite accompanied by the increase of calcium carbonate and increase of the amorphous phase contents different approaches were applied to identify and quantify educts and products. For quantitative phase analysis, PXRD with the Rietveld method [36] and differential scanning calorimetry with thermogravimetry (DSC-TG; STA 449 F3 Jupiter, Netzsch, Selb, Germany) coupled with mass spectrometer (MS; QMS 403D Aeolos Netzsch; atom mass units 1 to 50 u were recorded) and infrared spectroscopy (IR; Tensor II with TGA-IR extension compartment from Bruker, Karlsruhe, Germany) were used. The thermoanalytical measurements were carried out from ambient temperature (296 K) to 1273 K (1000 °C) with a heating rate of 10 K per minute. For the DSC-TG measurements ~15 to ~25 mg sample material per measurement were used.

With DSC-TG/IR/MS the amount of X-ray amorphous content of $CaCO_3$ in the product could be analyzed as well.

The content of carbonate was calculated from the mass loss associated with CO_2:

$$CaCO_3[\text{wt \%}] = \frac{\text{mass loss } CO_2 \text{ [wt \%]}}{\left(\frac{\text{mass } CO_2 \text{ [g/mol]}}{\text{mass } CaCO_3 \text{ [g/mol]}}\right)} \quad (2)$$

Microstructure of educts and products were characterized by SEM (JEOL JSM 6300 combined with X-Flash 5010 detector from Bruker; secondary electron pictures were taken with 15 keV; samples were sputtered with gold).

2.3. Experimental Setup

Carbonation of wollastonite at three different temperatures (296 K, 323 K, and 333 K) was investigated. As starting conditions 1 g sample material was mixed with 5 mL H_2O in the steel reactor. 20 mL CO_2 (5.5 MPa) were pumped by the ISCO-pump into the steel reactor, to obtain a pressure of 2 MPa inside the reactor. The temperature in steel reactors was adjusted by placing them in a drying chamber. For each temperature (296 K, 323 K, and 333 K) several experiments with different time intervals and constant pressure (2 MPa) were performed (Table 3).

Table 3. Overview of performed series of experiments at constant pressure and varied time and temperature.

Temperature (K)	Pressure (MPa)	Reaction Time (h)
296	2	0, 24, 48, 72, 96, 120, 144
323	2	0, 6, 18, 24, 48
333	2	0, 3, 6, 12, 18, 24

In addition, a series of experiments with constant time and temperature but varied pressure were performed. The applied pressure ranged from 0.2 MPa to 5 MPa (Table 4).

Table 4. Overview of performed series of experiments at varied pressure and constant time and temperature.

Temperature (K)	Pressure (MPa)	Reaction Time (h)
333	0.2, 0.5, 1.0, 1.5, 2.0, 2.6, 4.0, 5.0	6

To determine carbonation and reactions rates educts and products were analyzed by PXRD, DSC-TG/MS/IR and SEM.

3. Results and Discussion

The results of the quantification of the educts and products at different temperatures and pressures showed that temperature has a higher impact on the conversion of wollastonite to $CaCO_3$ than applied pressure.

3.1. Microstructure (SEM)

For the microscopic analysis of the morphology of educts and products SEM was used. The raw material exhibited wollastonite grains, showing elongated crystals of 5–6 µm × 10–12 µm (Figure 1, white arrows).

The carbonated wollastonite still showed small and elongated (2.5 × 5 µm) wollastonite (Wo) crystals, covered with carbonate crystals (Figure 2a, white arrow). Yet aggregates of carbonate crystals (Cb, Figure 2b, white arrow) were observed in the micrograph shown in Figure 2 (white arrow).

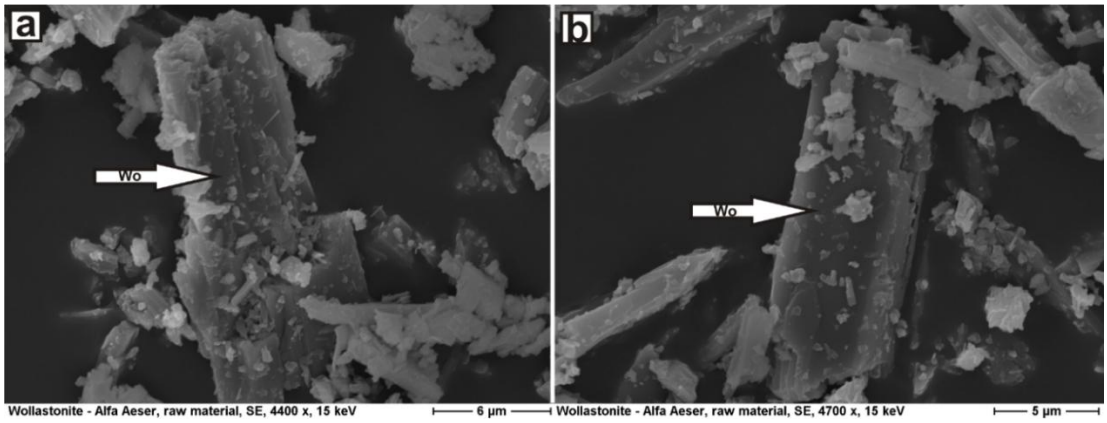

Figure 1. Secondary electron (SE) images of two elongated wollastonite grains (arrows, Wo). The grain on the left (**a**) is 6 × 12 µm, the grain on the right (**b**) 5 × 10 µm.

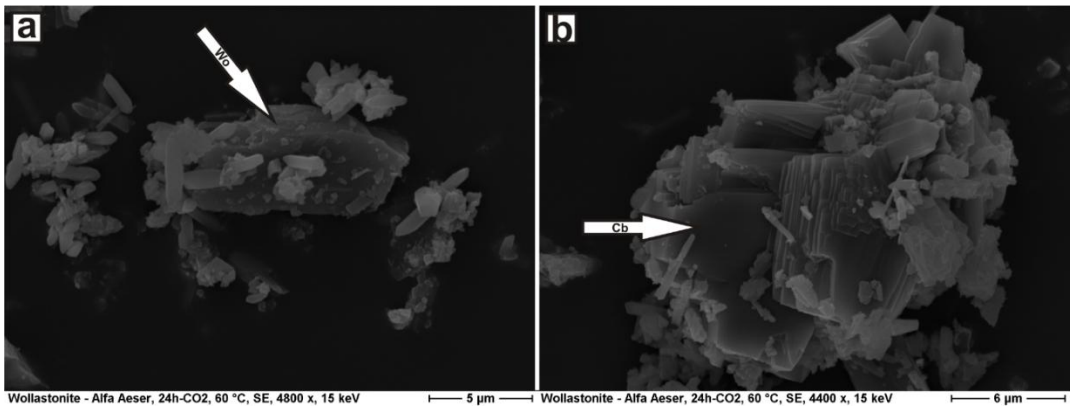

Figure 2. Secondary electron (SE) images of carbonated wollastonite. A wollstonite grain with small crystals of carbonate on the left (**a**, Wo). An aggregate of carbonate crystals on the right (**b**, Cb).

3.2. PXRD Analysis

To quantify the carbonation reaction of natural wollastonite (Table 5), samples were measured with PXRD before and after the CO_2 treatment. The results of the PXRD-analysis showed three crystalline phases (wollastonite, calcite, and aragonite) and an amorphous content, determined by adding 10 wt % of rutile as internal standard (Table 5 and Figures 3 and 4) in the starting material and the reaction products as well.

Table 5. Composition of the used raw material and carbonated wollastonite (24 h, 333 K), determined by powder X-ray diffraction (PXRD) and Rietveld refinement [38] ($Rwp_{Raw\ material}$: 7%, $Rwp_{carbonated\ wollastonite}$: 7%).

Phase	Raw Material	Carbonated Wollastonite
	Content (wt %)	Content (wt %)
Wollastonite	90 ± 1	4 ± 1
Calcite	5 ± 1	29 ± 1
Aragonite	1 ± 1	21 ± 1
Amorphous	4 ± 1	45 ± 1

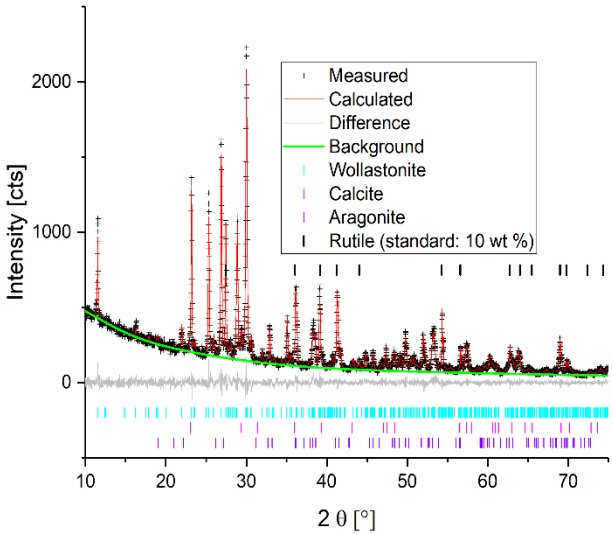

Figure 3. PXRD of Rietveld analysis [36–38] of the used raw material. Three crystalline phases and an amorphous content were determined by adding an internal TiO_2-standard of known weight: wollastonite (cyan), calcite (magenta) and aragonite (purple).

In Figure 4, the wollastonite with the fastest and most advanced conversion to carbonates (24 h, 333 K, 2 MPa) is shown. The results at the quantification of all carbonation reactions of wollastonite at 2 MPa is shown in part 3.4 of this study.

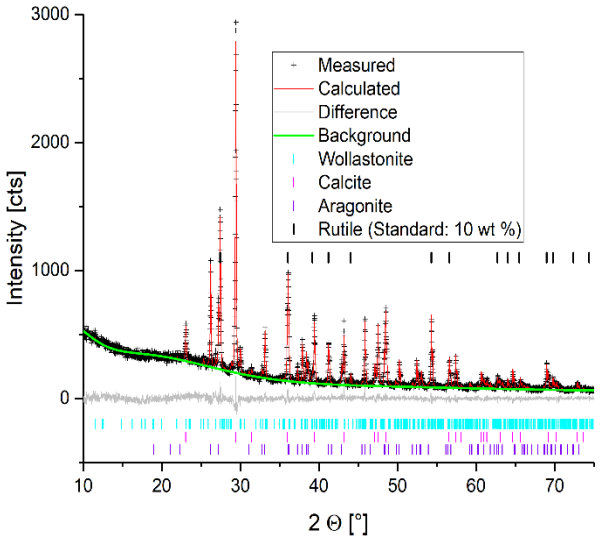

Figure 4. PXRD of Rietveld analysis [36–38] of carbonated wollastonite (carbonated at 333 K, 2 MPa, with 24 h reaction time). Three crystalline phases and an amorphous content were determined by adding an internal TiO_2-standard of known weight: wollastonite (cyan), calcite (magenta) and aragonite (purple).

3.3. DSC-TG/MS/IR Measurements

DSC-TG/MS/IR measurement of the raw material and the carbonated wollastonite were carried out to determine the entire content of water and carbonate in the material because X-ray amorphous carbonate could not be determined with PXRD, when additional amorphous phases (SiO_2) are also present in the mixtures.

DSC-TG/MS/IR measurements as shown in Figure 5 were performed with the raw material. During the measurement, the sample lost 2.1% of its weight. 1.7 wt % were associated with CO_2,

which results in original content of 3.9 wt % carbonate in the sample (Figure 5, Equation (2)). At the beginning of the experiment only H_2O were detected by mass spectrometry. The detected mass flow of H_2O (Figure 5, green line) decreased from 400 K to 800 K. From 800 K to 1050 K only CO_2 were measured by mass spectrometry. The mass flow of CO_2 reached its maximum at approximately 1000 K (Figure 5, magenta line). The measured weight loss (Figure 5, black line) decreased slowly from 400 K to 850 K. Starting with the increased mass flow of CO_2 the weight loss increased significantly (850 K to 1050 K). At temperatures higher than 1050 K, the mass of the sample did not change. The DSC-signal (Figure 5, blue line) showed amplitudes at 400 K and 1000 K, which were associated with the detected peaks of the mass flows of H_2O (400 K) and CO_2 (1000 K).

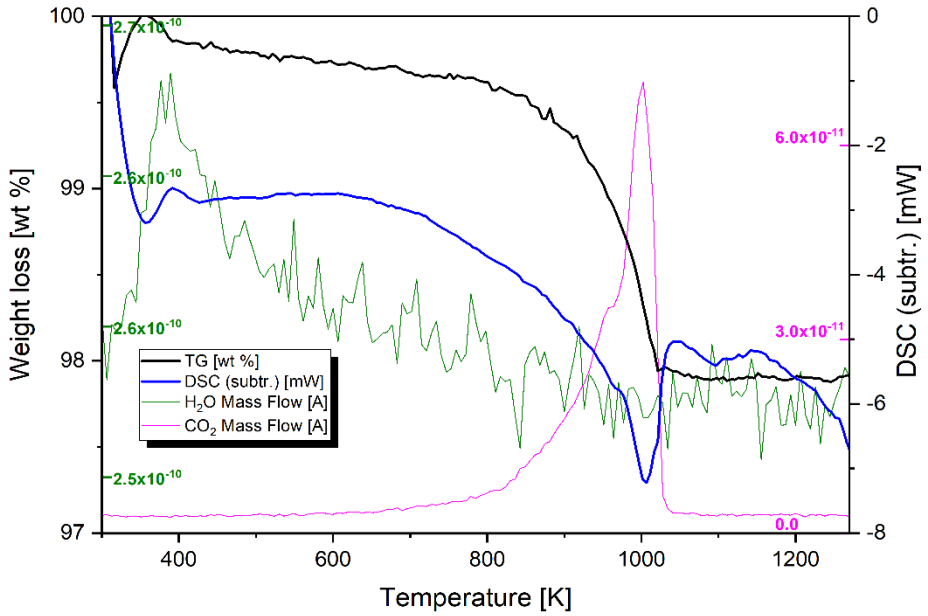

Figure 5. Result of the differential scanning calorimetry with thermogravimetry coupled with a mass spectrometer (DSC-TG/MS) measurement of wollastonite raw material (initial weight 20.3 mg). Measurement from 296 K to 1273 K with heating rate of 10 K/min. The weight loss (wt %) is shown by the black line and the DSC-signal (mW) by the blue line. The green line shows the mass flow (A) for H_2O, and the magenta line the mass flow (A) for CO_2.

The results of the Rietveld analysis and the DSC-TG measurements of the raw material for the content of carbonate were in good agreement (Rietveld: 5%; DSC-TG: 4%).

DSC-TG/MS/IR measurements on the carbonated wollastonite, shown exemplarily in Figure 6, were performed. During the measurement, the sample lost 25.4% of its weight. 23.9% were associated with CO_2, which resulted in original content of 54.8 wt % carbonate in the sample (Figure 6, Equation (2)). At approximately 400 K the mass spectrometer detected a peak of the mass flow of H_2O (Figure 6, green line). The mass flow decreased rapidly until 500 K was reached. From 500 K to 750 K the mass flow of H_2O rose again and held a plateau until 950 K. The IR analysis did also confirm the investigation of the releasing behavior of H_2O from $CaCO_3$. The mass flow of H_2O decreased significantly at temperatures higher than 950 K. The detection of the mass flow of CO_2 (Figure 6, magenta line) started at 800 K and increased slightly until 950 K was reached, then it formed a sharp peak until 1100 K was reached. At temperatures higher than 1100 K, the mass flow of CO_2 was nearly zero. The measured weight loss (Figure 6, black line) decreased slowly until 900 K. Starting with the increase of the mass flow of CO_2 the weight loss increased significantly (900 K to 1100 K). At temperatures higher than 1100 K, the mass of the sample did not change. The DSC-signal (Figure 6, blue line) showed a negative (endothermic) amplitude at 1100 K which was associated with the detected peak of the mass flow of CO_2. At 1150 K the DSC-signal showed a positive amplitude, which could be ascribed to the formation

of Ca_2SiO_4. PXRD-measurements were performed on the same sample which showed small contents of C_2S (larnite, i.e., Ca_2SiO_4).

The results of the Rietveld method and the DSC-TG measurements of the carbonated wollastonite for the content of carbonate were again in good agreement (Rietveld: 50%; DSC-TG: 55%).

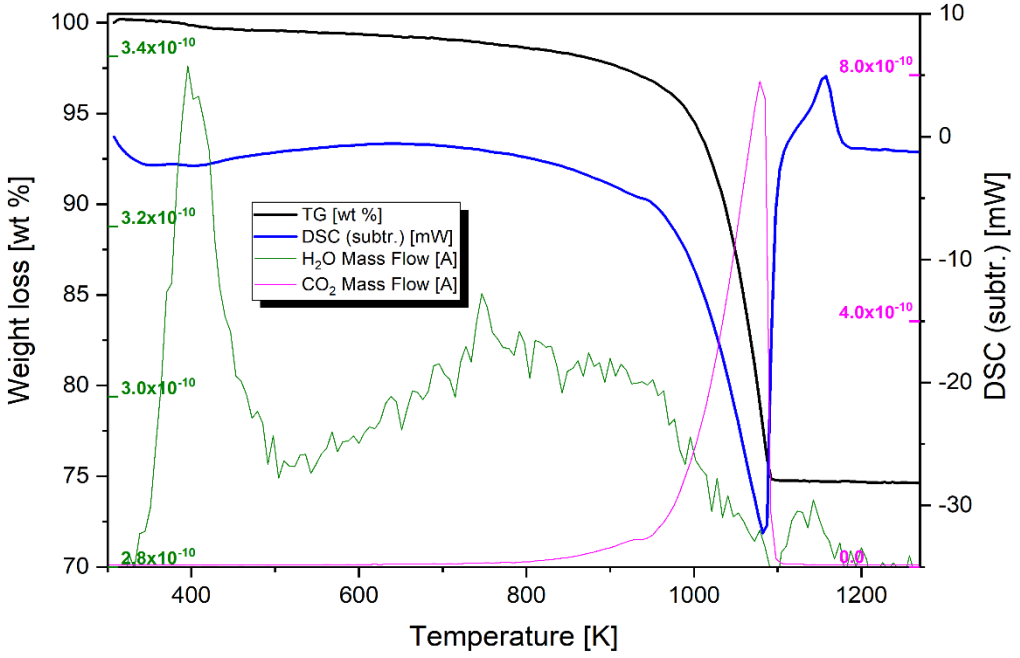

Figure 6. Result of the DSC-TG/MS measurement of carbonated (at 2 MPa and 333 K for 24 h) wollastonite (initial weight 15.2 mg). Measurement from 296 K to 1273 K with heating rate of 10 K/min. The weight loss (wt %) is represented by the black line, the DSC-signal (mW) by the blue line. The green line shows the mass flow (A) for H_2O, and the magenta line the mass flow (A) for CO_2.

3.4. Discussion of the PXRD and DSC-TG/MS Results

The results of the PXRD-measurements with the Rietveld method and the DSC-TG/MS/IR-measurements were collected and plotted in three diagrams (Figures 7–9). The quantity of the phases wollastonite (black squares), amorphous (blue triangles), calcite (magenta circles) and aragonite (green circles) were determined by the Rietveld method. The red circles symbolized the sum of calcite and aragonite and therefore the content of carbonate in the sample detected by PXRD. The amount of $CaCO_3$ determined by TG measurements were shown by cyan circles.

In Figure 7, the carbonation of wollastonite at 296 K is shown with seven different reaction times. To show the good reproducibility several experiments were performed two times (Figure 7). At 296 K, the reaction was not completed after 144 h. The content of calcite (magenta circles), the amount of $CaCO_3$ determined by TG measurements (cyan circles) and of the amorphous content (blue triangles) in the sample increased exponentially while the content of wollastonite (black squares) decreased similarly. No further aragonite (green circles) was formed (Figure 7).

At 323 K, a high degree of conversion (>90%) was already achieved after 48 h (Figure 8). The content of calcite (magenta circles), aragonite (green circles), the amount of $CaCO_3$ determined by TG measurements (cyan circles) and the amorphous content (blue triangles) increased exponentially, while the content of wollastonite (black squares) decreased exponentially in an analog manner. At 24 h, the contents of calcite and aragonite almost reached the same amount (~20 wt %), while at the beginning of the experiment the content of calcite was higher (Figure 8, grey circles marked by arrows).

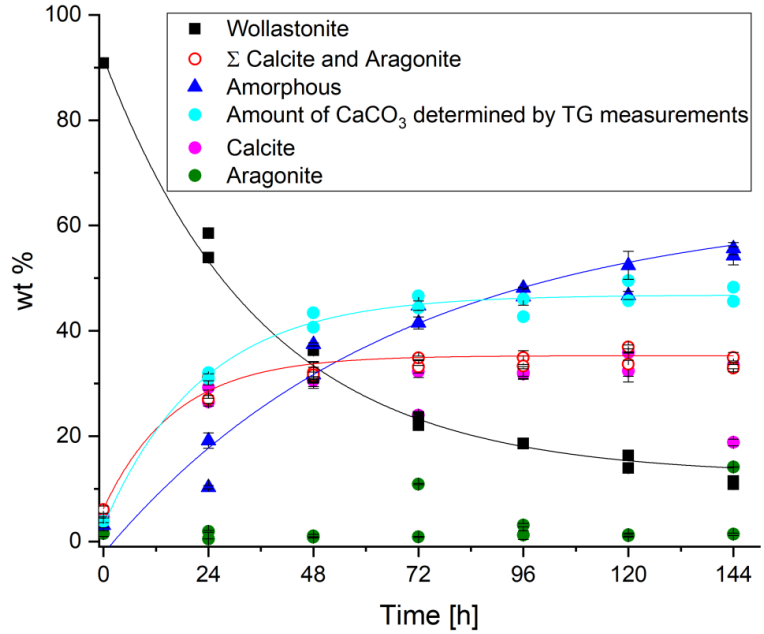

Figure 7. Carbonation of wollastonite at 296 K (23 °C, ambient), 2 MPa and aqueous conditions (H_2O). The quantity of the phases wollastonite (black squares), amorphous (blue triangles), calcite (magenta circles) and aragonite (green circles) were determined by the Rietveld method. The red circles symbolize the sum of calcite and aragonite and therefore the content of carbonate in the sample detected by PXRD. The amount of $CaCO_3$ determined by TG measurements are symbolized by cyan circles.

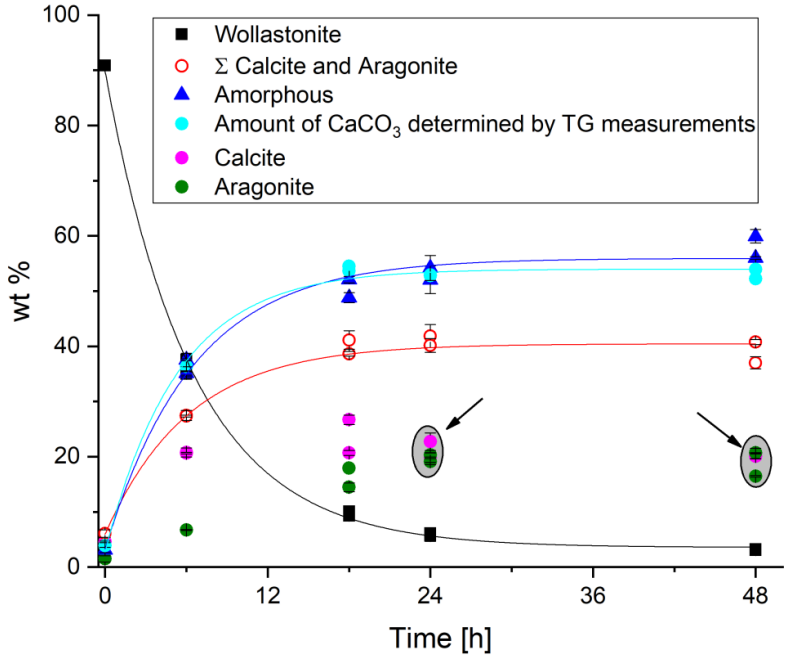

Figure 8. Carbonation of wollastonite at 323 K (50 °C), 2 MPa and aqueous conditions (H_2O). The quantity of the phases wollastonite (black squares), amorphous (blue triangles), calcite (magenta circles) and aragonite (green circles) were determined by the Rietveld method. The red circles symbolize the sum of calcite and aragonite and therefore the content of carbonate in the sample detected by PXRD. The amount of $CaCO_3$ determined by TG measurements are symbolized by cyan circles. The ellipsoids with arrows depict the symbols, at which aragonite and calcite exhibite nearly the same amount.

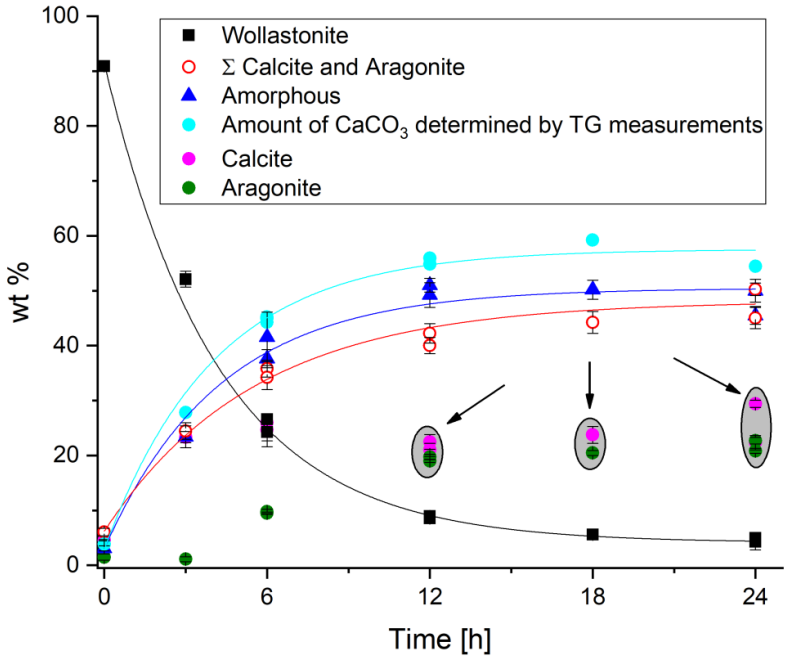

Figure 9. Carbonation of wollastonite at 333 K (60 °C), 2 MPa and aqueous conditions (H_2O). The quantity of the phases wollastonite (black squares), amorphous (blue triangles), calcite (magenta circles) and aragonite (green circles) were determined by the Rietveld method. The red circles symbolize the sum of calcite and aragonite and therefore the content of carbonate in the sample detected by PXRD. The amount of $CaCO_3$ determined by TG measurements are symbolized by cyan circles. The ellipsoids with arrows depict the symbols, at which aragonite and calcite exhibit nearly the same amount.

At 333 K, the conversion was nearly completed already after 24 h (Figure 9). The contents of calcite (magenta circles), aragonite (green circles) and the total amount of $CaCO_3$ determined by TG measurements (cyan circles) and the amorphous content (blue triangles) increased exponentially, while the content of wollastonite (black squares) decreased exponentially. At 12 h the contents of calcite and aragonite almost reached the same amount (~20 wt %) whereas at the beginning (6 h and 18 h) of the experiment the content of calcite was higher (Figure 9, grey circles marked by arrows).

At each investigated temperature (296 K, 323 K, 333 K), an exponentially decrease of wollastonite was observed. This was also true for the increase of calcite and the amorphous content vice versa. At higher temperatures (323 K and 333 K), aragonite exhibited also exponential increase (Figures 8 and 9).

An additional experiment was performed, in which the temperature (333 K) and time (6 h) were held constant and only the pressure varied. The results showed that the reaction was mostly independent of pressure (Figure 10).

At low pressure (0.2 MPa) the decrease of wollastonite was slower and newly formed aragonite was not observed. At higher pressures (>1 MPa) the carbonation of natural wollastonite showed no further dependence of the applied pressure (Figure 10). From 1 MPa to 5 MPa no differences considering the rate of wollastonite transformation were observed. However the formation of aragonite was dependent on pressure. From 0.2 MPa to 2 MPa the formation of aragonite increased, from 2 MPa to 4 MPa it was constant and from 4 MPa to 5 MPa the formation of aragonite decreased. Figure 11 shows this observation as normalized amount of the wollastonite conversion.

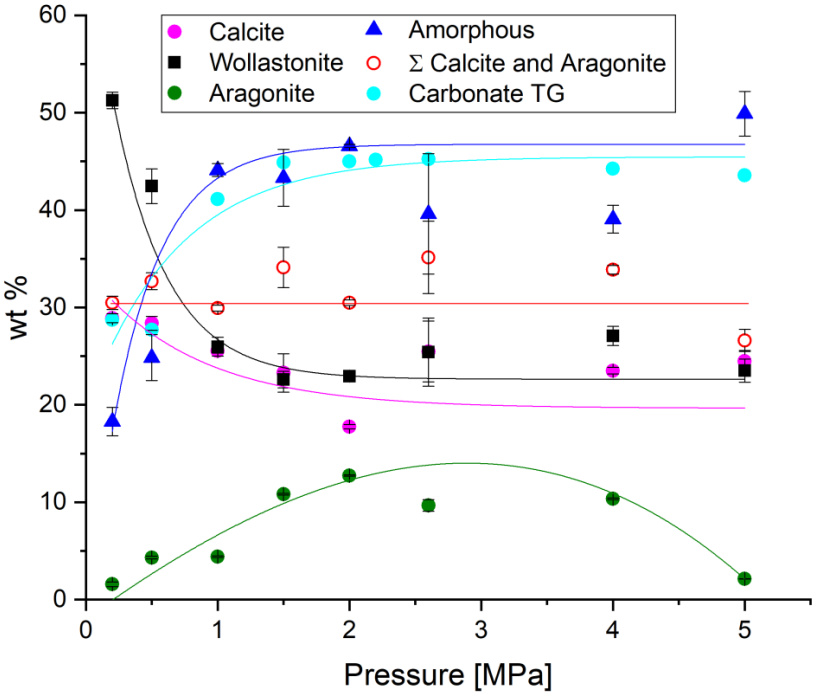

Figure 10. Carbonation of wollastonite at 333 K (60 °C), aqueous conditions (H_2O) and reaction time of 6 h. The pressure was varied from 0.2 MPa to 5 MPa. The quantity of the phases wollastonite (black squares), amorphous (blue triangles), calcite (magenta circles) and aragonite (green circles) were determined by the Rietveld method. The red circles symbolized the sum of calcite and aragonite and therefore the content of carbonate in the sample detected by PXRD. The amount of $CaCO_3$ determined by TG measurements were symbolized by cyan circles.

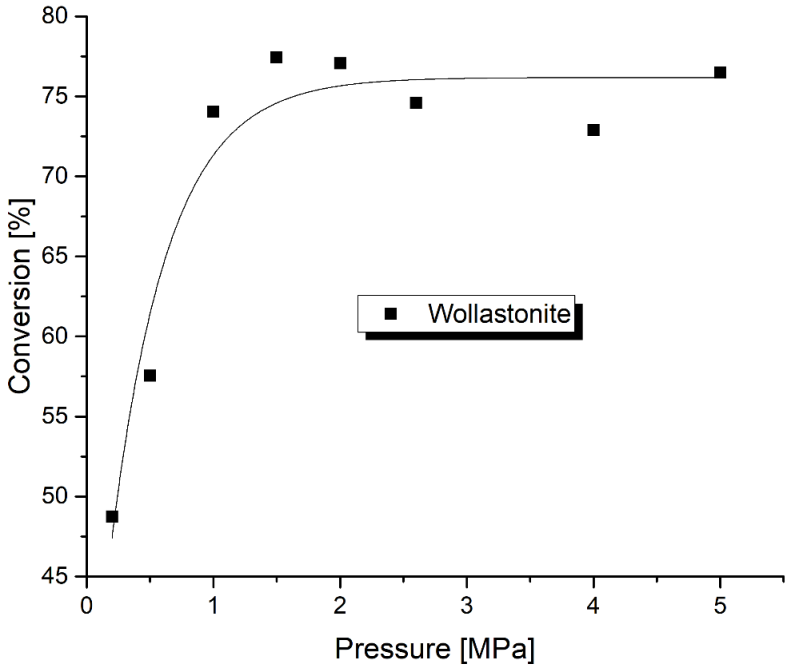

Figure 11. Conversion rate of wollastonite at different pressures and constant temperature (333 K) and time (six hours).

Considering the conversion of wollastonite to $CaCO_3$ in the presence of water the reaction rate of the carbonation depended strongly on the temperature, at higher temperatures the reaction rate was significantly higher (Figures 7–9).

A first order reaction was assumed because the reaction was only dependent on wollastonite. The amount of CO_2 was one order of magnitude higher than the amount of wollastonite. This assumption could be supported by plotting ln (C) vs time (Figure 12) from which a linear dependency after a conversion of ~90% could be derived.

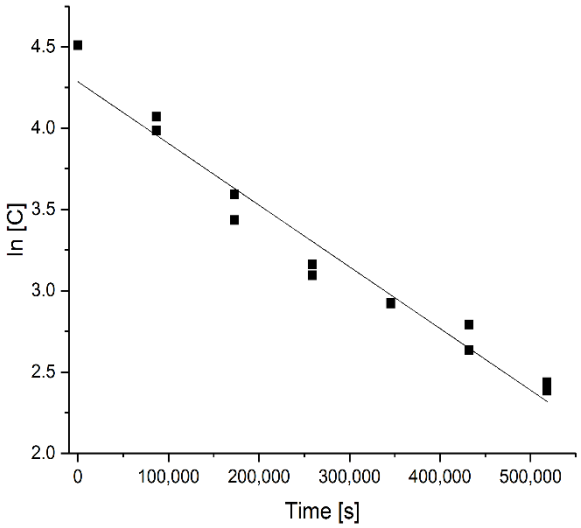

Figure 12. Conversion rate of wollastonite plotted as ln (C) vs time.

In Figure 13 the wollastonite hkl reflection (100) at 12 ° 2Θ decreased from 296 K to 333 K.

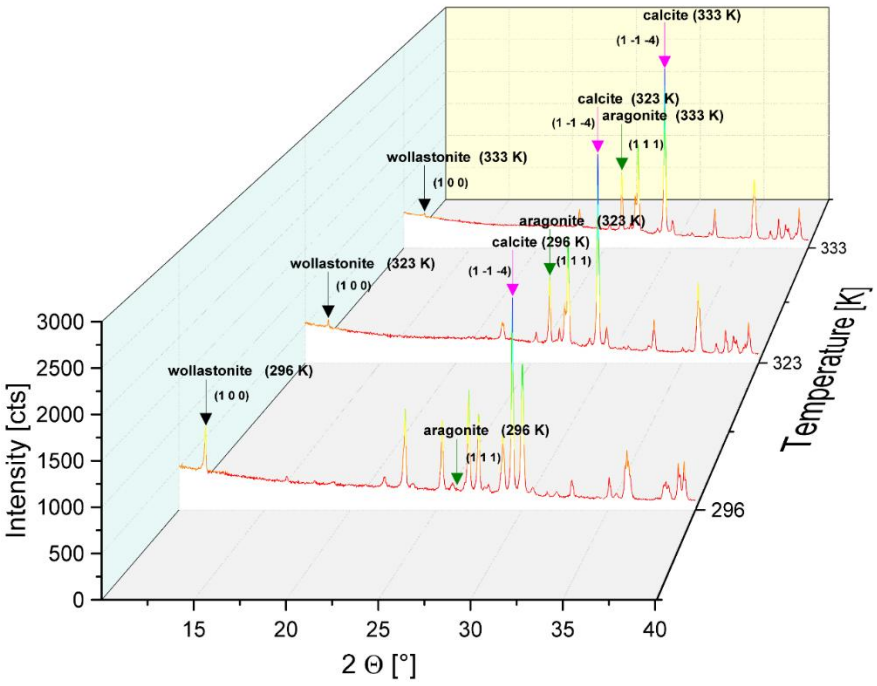

Figure 13. X-ray powder diffractograms of carbonated wollastonite, recorded at different temperatures (296 K, 323 K, 333 K). Pressure (2 MPa) and time (24 h) were constant. The carbonation rate increases at higher temperatures.

Considering the conversion rates from wollastonite to calcite the rate constants and activation energies could be estimated (Table 6).

Table 6. Rate constants k and activation energies E_A of $CaSiO_3/CaCO_3$ conversion.

Activation Energies	Rate Constants	kJ/mol
E_A (323–296 K)	$-3.79 \times 10^{-6} \pm 2.36 \times 10^{-7}$	63.88 ± 0.2
E_A (333–296 K)	$-3.32 \times 10^{-5} \pm 1.87 \times 10^{-6}$	58.88 ± 0.6
E_A (333–323 K)	$-5.42 \times 10^{-5} \pm 1.95 \times 10^{-6}$	43.70 ± 2.0

The carbonation reaction of wollastonite starts at the surface of a grain and moves towards the center [10,11,34]. The reaction rate will decrease because of the growing layer thickness of $CaCO_3$ between unreacted $CaSiO_3$ and CO_2. Consequently, low amounts (5% to 10%) of material will remain unreacted within experimental periods. At 323 K, the reaction rate is three times faster, whereas at 333 K the reaction rate increased by a factor of six (Figure 14). The values of the activation energy E_A for the carbonation reaction ranged from 44 to 64 kJ·mol^{-1} (Table 6) depending on ΔT, with the latter being in a good agreement with the results reported in Brady [39] (~72 kJ·mol^{-1}).

The carbonation rate of wollastonite at different temperatures (when ~10% of wollastonite were still present) showed a non-linear behavior (exponential decrease) of reaction time (Figure 14).

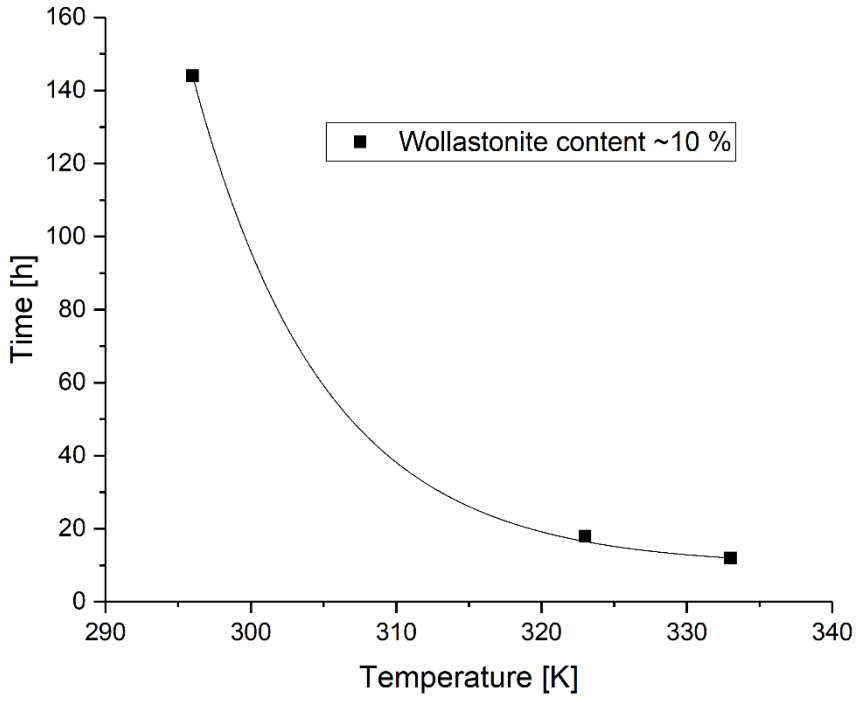

Figure 14. Carbonation rate of wollastonite at different temperatures at varying reaction times. Higher temperature resulted in a faster carbonation rate. The reaction time showed a non-linear behavior (data points were fitted with an exponential function).

The p-T conditions in the steel reactor were thermodynamically not suitable [40] for the formation of aragonite. Although metastable aragonite formation can be stabilized in presence of Sr [41], the content of Sr in the material was very low (0.01 wt %). Despite in preliminary performed experiments no aragonite was formed when the carbonate was previously removed from the raw material. Therefore, it was assumed that the small content of aragonite in the raw material functioned as a seed crystal for further metastable aragonite growth.

4. Conclusions

Experiments considering the conversion of $CaSiO_3$ to $CaCO_3$ in aqueous conditions were performed at different temperatures and pressures. The kinetics of this reaction was strongly dependent on temperature (Figure 13). Pressure seemed not to be critical for reaction kinetics (Figures 10 and 11). The degree of conversion, i.e., the amount of reaction products (amorphous and crystalline), could be determined by XRD and coupled DSC-TG/MS/IR analysis. Calcite, aragonite and amorphous $CaCO_3$ and amorphous SiO_2 were observed. Depending on the temperature a nearly complete reaction was achieved within the experimental periods of 1–144 h. Activation energies E_A could be determined and were in better agreement with the values reported by Brady [39] compared to those given by Huijgen (22 kJ·mol^{-1} at <38 µm, 20 kJ·mol^{-1} at <106 µm, 16 kJ·mol^{-1} at <500 µm) [32].

At the defined conditions (333 K, 2 MPa) relevant for the point of injection of CO_2, the carbonation reaction of wollastonite was already completed after 24 h (Figure 9). At lower temperatures, the carbonation reaction was rather slow (144 h at 296 K, Figure 7 and 48 h at 323 K, Figure 8). Hence, it could be proven that the use of wollastonite as a cementitious material suitable for sealing the borehole in CCS is applicable.

To characterize mineral association and their stability as well, the reaction at the interfaces between rocks and casing materials, more experiments at selected pressure, temperature and composition of formation waters will be performed. The long-term stability is still under investigation. As anticipated, the most likely application of wollastonite as cement in CCS would be for sealing the well after injection of CO_2 in the reservoir. In that case, the wollastonite will be mixed with water and pumped into the well like conventional cement, mortar or concrete. The CO_2 stored in the reservoir will cause the hardening and therefore the sealing of the borehole.

Acknowledgments: We want to thank the German Federal Ministry for Economic Affairs and Energy (BMWi; FKZ: 03ET7031D) for financial support and Sabine Walther for sample preparation and support on the SEM. The constructive comments and helpful suggestions of two anonymous reviewers are gratefully acknowledged. We acknowledge the financial support within the funding program Open Access Publishing by the German Research Foundation (DFG).

Author Contributions: The authors worked together in a research project. Herbert Pöllmann, Andreas Neumann, Kristoff Svensson and Christof Lempp conceived and designed the experiments. Kristoff Svensson and Andreas Neumann performed the experiments. Kristoff Svensson and Andreas Neumann analyzed the data. Kristoff Svensson, Andreas Neumann, Flora Feitosa Menezes, Herbert Pöllmann and Christof Lempp contributed ideas, knowledge and discussion. Kristoff Svensson, Andreas Neumann and Herbert Pöllmann wrote the Paper.

Conflicts of Interest: The authors declare no conflict of interest. The founding sponsors had no role in the design of the study; in the collection, analyses, or interpretation of data; in the writing of the manuscript, and in the decision to publish the results.

References

1. NOAA (National Oceanic and Atmospheric Administration); Earth System Research Laboratory. Trends in Atmospheric Carbon Dioxide. Available online: https://www.esrl.noaa.gov/gmd/ccgg/trends/ (accessed on 18 December 2017).
2. Benson, S.M.; Orr, F.M., Jr. Carbon Dioxide Capture and Storage. *MRS Bull.* **2008**, *33*, 303–305. [CrossRef]
3. Locher, F. *Zement–Grundlagen der Herstellung und Verwendung*, 1st ed.; Verlag Bau+Technik GmbH: Düsseldorf, Germany, 2000; p. 522, ISBN 978-3-7640-0400-2.
4. Taylor, H.F.W. *Cement Chemistry*, 2nd ed.; Thomas Telford Publishing, Thomas Telford Services Ltd.: London, UK, 1997; p. 459, ISBN 0-7277-2592-0.
5. Pöllmann, H. Mineralogical strategies to reduce CO_2 in the fabrication of alternative cements. *Ibausil Conf. Rep.* **2015**, *1*, 111–129.
6. Rice, J.; Ferry, J. Buffering, Infiltration, and the Control of Intensive Variables during Metamorphism. *Rev. Miner. Geochem.* **1982**, *10*, 263–326.
7. Svensson, K.; Neumann, A.; Pöllmann, H.; Menezes, F.; Lempp, C. Curing by carbonatisation of Wollastonite. *GDCh–Tag. Bauchem.* **2017**, *52*, 80–83.
8. CLUSTER. Joint Research Project CLUSTER. Available online: www.bgr.bund.de/CLUSTER/ (accessed on 18 December 2017).

9. Gartner, E.; Hirao, H. A review of alternative approaches to the reduction of CO_2 emissions associated with the manufacture of the binder phase in concrete. *Cem. Concr. Res.* **2015**, *78*, 126–142. [CrossRef]
10. Vilani, C.; Spragg, R.; Tokpatayeva, R.; Olek, J.; Weiss, W. Characterizing the Pore Structure of Carbonated Natural Wollastonite. In Proceedings of the 4th International Conference on the Durability of Concrete Structures, West Lafayette, IN, USA, 24–26 July 2014.
11. Sahu, S.; DeCristofaro, N. *Solidia Cement^{TM}–Part One of a Two-Part Series Exploring the Chemical Properties and Performance Results of Sustainable Solidia Cement^{TM} and Solidia Concrete^{TM}*; Solidia Technologies: Piscataway, NJ, USA, 2013; pp. 1–12.
12. Abbasi, E.; Hassanzadeh, A.; Abbasian, J. Regenerable MgO-based surbent for high temperature CO_2 removal from syngas: 2. Two-zone variable diffusivity shrinking core model with expanding product layer. *Fuel* **2013**, *105*, 128–134. [CrossRef]
13. Longo, R.C.; Cho, K.; Brüner, P.; Welle, A.; Gerdes, A.; Thissen, P. Carbonation of Wollastonite(001) Competing Hydration: Microscopic Insights from Ion Spectroscopy and Density Dunctional Theory. *Am. Chem. Soc. Appl. Mater. Interfaces* **2015**, *7*, 4706–4712. [CrossRef] [PubMed]
14. Shi, Z.; Lothenbach, B.; Geiker, M.R.; Kaufmann, J.; Leemann, A.; Ferreiro, S.; Skibsted, J. Experimental studies and thermodynamic modeling of the carbonation of Portland cement, metakaolin and limestone mortars. *Cem. Concr. Res.* **2016**, *88*, 60–72. [CrossRef]
15. Abdoulghafour, H.; Gouze, P.; Luquot, L.; Leprovost, R. Characterization and modeling of the alteration of fractured class-G Portland cement during flow of CO_2-rich brine. *Int. J. Greenh. Gas Control* **2016**, *48*, 155–170. [CrossRef]
16. Luquot, L.; Abdoulghafour, H.; Gouze, P. Hydro-dynamically controlled alteration of fractured Portland cements flowed by CO_2-rich brine. *Int. J. Greenh. Gas Control* **2013**, *16*, 167–179. [CrossRef]
17. Ozyurtkan, M.H.; Radonjic, M. An experimental study of the effect of CO_2 rich brine on artificially fractured well-cement. *Cem. Concr. Compos.* **2014**, *45*, 201–208. [CrossRef]
18. Yalcinkaya, T.; Radonjic, M.; Willson, C.; Bachu, S. Experimental Study on a Single Cement-Fracture Using CO_2 Rich Brine. *Energy Procedia* **2011**, *4*, 5225–5342. [CrossRef]
19. Carey, W.J.; Svec, R.; Grigg, R.; Zhang, J.; Crow, W. Experimental investigation of wellbore integrity and CO_2-brine flow along casing-cement microannulus. *Int. J. Greenh. Gas Control* **2010**, *4*, 272–282. [CrossRef]
20. Barlet-Gouédard, V.; Rimmelé, G.; Porcherie, O.; Quisel, N.; Desroches, J. A solution against well cement degradation under CO_2 geological storage environment. *Int. J. Greenh. Gas Control* **2009**, *3*, 206–216. [CrossRef]
21. Wigand, M.; Kaszuba, J.P.; Carey, W.J.; Hollis, K.W. Geochemical effects of CO_2 sequestration on fractured wellbore cement at the cement/caprock interface. *Chem. Geol.* **2009**, *265*, 122–133. [CrossRef]
22. Nakano, K.; Ohbuchi, A.; Mito, S.; Xue, Z. Chemical interactionof well composite samples with supercritical CO_2 along the cement–sandstone interface. *Energy Procedia* **2014**, *63*, 5754–5761. [CrossRef]
23. Zhang, L.; Dzombak, D.A.; Nakles, D.V.; Hawthorne, S.B.; Miller, D.J.; Kutchko, B.G.; Lopano, C.L.; Strazisar, B.R. Characterization of pozzolan-amended wellbore cement exposed to CO_2 and H_2S gas mixtures under geologic carbon storage conditions. *Int. J. Greenh. Gas Control* **2013**, *19*, 358–368. [CrossRef]
24. Zhang, L.; Dzombak, D.A.; Nakles, D.V.; Hawthorne, S.B.; Miller, D.J.; Kutchko, B.G.; Lopano, C.L.; Strazisar, B.R. Rate of H_2S and CO_2 attack on pozzolan-amended Class H well cement under geologic squestration conditions. *Int. J. Greenh. Gas Control* **2014**, *27*, 299–308. [CrossRef]
25. Mito, S.; Xue, Z.; Satoh, H. Experimental assessment of well integrity for CO_2 geological storage: Batch experimental results on geochemical interactions between a CO_2-brine mixture and a sandstone-cement-steel sample. *Int. J. Greenh. Gas Control* **2015**, *39*, 420–431. [CrossRef]
26. Wolterbeek, K.T.; Hangx, S.J.T.; Spiers, C.J. Effect of CO_2-induced reactions on the mechanical behaviour of fractured wellbore cement. *Geomech. Energy Environ.* **2016**, *7*, 26–46. [CrossRef]
27. Kutchko, B.G.; Strazisar, B.R.; Hawthorne, S.B.; Lopano, C.L.; Miller, D.J.; Hakala, A.J.; Guthrie, G.D. H_2S-CO_2 reaction with hydrated Class H well cement: Acid-gas injection and CO_2 Co-sequestration. *Int. J. Greenh. Gas Control* **2011**, *5*, 880–888. [CrossRef]
28. Bube, C.; Metz, V.; Bohnert, E.; Garbev, K.; Schild, D.; Kienzler, B. Long-Term cement corrosion in chloride-rich solutions relevant to radioactive waste disposal in rock salt–Leaching experiments and thermodynamic simulations. *Phys. Chem. Earth* **2013**, *64*, 87–94. [CrossRef]

29. Jain, J.; Deo, O.; Sahu, S.; DeCristofaro, N. *Solidia Cement^{TM}–Part Two of a Series Exploring the Chemical Properties and Performance Results of Sustainable Solidia Cement^{TM} and Solidia Concrete^{TM}*; Solidia Technologies: Piscataway, NJ, USA, 2014; pp. 1–17.
30. Jain, J.; Atakan, V.; DeChristofaro, N.; Jeong, H.; Olek, J. *Performance of Calcium Silicate-based Carbonated Concretes vs. Hydrated Concretes under Freeze-thaw Environments*; Solidia Technologies: Piscataway, NJ, USA, 2015; pp. 1–8.
31. Ashraf, W.; Olek, J.; Atakan, V.; Hyungu, J. Effects of High Temperature on Carbonated Calcium Silicate Cement (CSC) and Ordinary Portland Cement (OPC) Paste. In Proceedings of the 5th International Conference on Durability of Concrete Structures, Shenzhen, China, 30 June–1 July 2016.
32. Huijgen, W.J.J.; Witkamp, G.-J.; Comans, R.N.J. Mechanisms of aqueous wollastonite carbonation as a possible CO_2 sequestration process. *Chem. Eng. Sci.* **2006**, *61*, 4242–4251. [CrossRef]
33. Daval, D.; Martinez, I.; Corvisier, J.; Findling, N.; Goffé, B.; Guyot, F. Carbonation of Ca-bearing silicates, the case of wollastonite: Experimental investigations and kinetic modeling. *Chem. Geol.* **2009**, *262*, 262–277. [CrossRef]
34. Min, Y.; Li, Q.; Voltolini, M.; Kneafsey, T.; Jun, Y.-S. Wollastonite Carbonation in Water-Bearing Supercritical CO_2: Effects of Particle Size. *Environ. Sci. Technol.* **2017**, *51*, 13044–13053. [CrossRef] [PubMed]
35. Degen, T.; Sadki, M.; Bron, E.; König, U.; Nénert, G. The Highscore suite. *Powder Diffr.* **2014**, *29*, 13–18. [CrossRef]
36. Rietveld, H.M. A profile refinement method for nuclear and magnetic structures. *J. Appl. Crystallogr.* **1969**, *2*, 65–71. [CrossRef]
37. Döbelin, N.; Kleeberg, R. Profex: A graphical user interface for the Rietveld refinement program BGMN. *J. Appl. Crystallogr.* **2015**, *48*, 1573–1580. [CrossRef] [PubMed]
38. Bergmann, J.; Friedel, P.; Kleeberg, R. BGMN–A new fundamental parameters based Rietveld program for laboratory X-ray sources, it's use in qualitative analysis and structure investigations. *Comm. Powder Diffr. Int. Union Crystallogr. CPD Newsl.* **1998**, *20*, 5–8.
39. Brady, P.V. The Effect of Silicate Weathering on Global Temperature and Atmospheric CO_2. *J. Geophys. Res.* **1991**, *96*, 18101–18106. [CrossRef]
40. Salje, E.; Viswanathan, K. The Phase Diagram Calcite-Aragonite as Derived from the Crystallographic Properties. *Contrib. Mineral. Petrol.* **1976**, *55*, 55–67. [CrossRef]
41. Sunagawa, I.; Takahashi, Y.; Imai, H. Strontium and aragonite-calcite precipitation. *J. Mineral. Petrol. Sci.* **2007**, *102*, 174–181. [CrossRef]